SAÜ Fen Bil Der 20. Cilt, 2.Sayı, s. 371-381, 2016

Investigation of nano metal and metal oxide particles synthesis by using medium frequency-induction method

Levent Kartal*[1], Yasin Kılıç[2], Güldem Kartal Şireli[3], Servet Timur[4]

13.10.2015 Geliş/Received, 08.06.2016 Kabul/Accepted

ABSTRACT

Synthesis of Ag, Fe_2O_3 and TiO_2 was investigated in medium frequency induction system to determine ideal conditions for the particle production with desired size. A high frequency ultrasonic generator was attached to induction furnace to synthesize particles from solutions of $AgNO_3$, $FeCl_3$, titanium tetra iso-propoxide (TTIP). Experiments were carried out under concentrations of 0.1 M, 0.01 M at constant parameters; 15 min. time, 800 ºC temperature, 1.0 L/min. flow rate. X-ray diffraction (XRD) studies confirmed the particle formation without contamination. Scanning electron microscopy (SEM) examinations revealed that size of particles were in the range of 50 nm to 400 nm.

Keywords: nanoparticle, titanium dioxide, iron oxide, silver, medium frequency induction

Orta frekans indüksiyon yöntemi ile nano-metal ve nano-metal oksit partikül sentezinin incelenmesi

ÖZ

Bu çalışmada, gümüş (Ag), demir oksit (Fe_2O_3) ve titanyum dioksit (TiO_2) partiküllerinin nano- boyutta üretimleri için gerekli şartlar, orta frekanslı indüksiyon partikül üretim sisteminde incelenmiştir. Partikül üretim sistemi; orta frekanslı indüksiyon fırını ile yüksek frekans ultrasonik atomizerin birleştirilmesi ile oluşturulmuştur. Bahsi geçen nano-partiküllerin üretimi 0,1 M ve 0,01 M konsantrasyonların da $AgNO_3$, $FeCl_3.6H_2O$, Titanyum tetra izopropoksit (TTIP) başlangıç malzemeleri kullanılarak gerçekleştirilmiştir. Deneyler, sabit 800 ºC reaksiyon sıcaklığı, 1.0 L/dk. taşıyıcı gaz debisi ve 15 dk. deney süresi şartlarında yapılmıştır. XRD ve SEM kullanılarak karakterize edilen nano-partiküllerin safsızlık içermediği ve 50 nm ile 400 nm arasında değişen boyutlarda oldukları görülmüştür.

Anahtar Kelimeler: nanopartikül, titanyum dioksit, demir oksit, gümüş, orta frekans indüksiyon

* Sorumlu Yazar / Corresponding Author

1 ITU, Chemical and Metallurgical Engineering, Metallurgical and Materials Eng., Istanbul - kartall@itu.edu.tr

2 ITU, Chemical and Metallurgical Engineering, Metallurgical and Materials Eng., Istanbul - kilicyas@itu.edu.tr

3 ITU, Chemical and Metallurgical Engineering, Metallurgical and Materials Eng., Istanbul - kartalgu@itu.edu.tr

4 ITU, Chemical and Metallurgical Engineering, Metallurgical and Materials Eng., Istanbul - timur@itu.edu.tr

1. INTRODUCTION

Nanoparticles exhibit very interesting electronic, magnetic, optical and chemical properties which are directly related to the shape, size, composition, and structure of synthesized powders [1,2]. For this reason, production of nanoparticles with controlled morphology and size distribution is very critical to meet the demand of required function. So far, many techniques have been developed to synthesize metal and metal oxide nanoparticles with uniform form and proportion including; laser ablation [3], RF thermal plasmas [4], flame synthesize [5], sol-gel [6], chemical vapor synthesis (CVS) [7], mechanical attrition [8] and spray pyrolysis [9], and etc.

Silver, titanium dioxide and iron oxide are the most investigated ones due to their unique properties. The main request of silver nanoparticles is for antibacterial applications; however, they potentially found utilizations in many different industries including food, paints, cosmetics, medical devices, catalysis, and so on. [10, 11]. Table 1 summarizes the previous reports on the control of the morphology and size of silver particles using the precursor types and precursor concentration in different spray pyrolysis methods [12-19]. As seen in Table 1, the particle sizes highly depend on the precursor concentration (i.e., the lower precursor concentration the smaller particle size) [15–19].

Table 1. Previous experimental results of silver particles synthesized by different spray pyrolysis methods

Morphology	Particle size, nm	Precursor salt/solvent	Precursor concentration (M and wt.%)	Heating temperature (°C)	References
Spherical	144-1000	$AgNO_3$/DI water	0.05-0.2 M	150 -1000	Stopic et al. [12]
	<20	$AgNO_3$/DI water	1.0×10^{-7} M	800	Pingali et al. [13]
	95-328	Ag Acetate	1 wt.%	400–800	Shih et al. [14]
	210-525	$AgNO_3$/DI water	0.05−0.4 M	200-800	Ebin et al. [15]
	50	$AgNO_3$, $Mg(NO3)_2$	40 wt.% $AgNO_3$ and $Mg(NO_3)_2$	740-790	Shi et al. [16]
	16 -53	$AgNO_3$/DI water	0.0235 -0.376M	1000	Zhang et al. [17]
	6-10	$AgNO_3$/DI water	0.1 M	200-600	Lee et al. [18]
	5-20	$AgNO_3$/DI water	0.1 M	200-600	Kim et al. [19]

Titanium dioxide is typically used as a pigment because of its high refractive index. Although this is one of the most common demands of titanium dioxide, interest for other implementations has increased tremendously; especially in waste water treatment, air purification, self-cleaning paints and solar cells [20-23]. The previous studies on the titanium oxide particles produced by different spray pyrolysis given in Table 2 [24-27] revealed that the concentration of the precursor is the most effective parameters on the titanium oxide particles production via spray pyrolysis and the average size of the powders are tuneable easily via altering the concentration of the precursors.

Table 2. Previous reported results of titanium oxide particles synthesized by different spray pyrolysis methods

Morpho logy	Particle size, nm	Precursor salt	Precursor concentration (M)	Heating temperature (°C)	References
Spherica l	390-706	TTIP, TC-300® and TC-400®,/DI water	0.01-0.1	500-900	Wang et al. [24]
	370–500	$TiCl_4$	-	150–800	Dugandzic et al. [25]
	28-70	TTIP/DI water	1.1×10^{-7}- 6.4×10^{-7}	100-500	Moravec et al. [26]
	100-400	Tetra-n-butyl orthotitanate ($C_{16}H_{36}O_4Ti$)	-	800	Bogovic, et al. [27]

Iron oxide nanoparticles are currently in the use of vitro diagnostics for decades due to their biocompatible properties. Moreover, these nanoparticles offer many potential applications namely, catalytic materials, waste water treatment adsorbents, pigments, gas sensors, ion exchangers, coatings, magnetic data storage devices [28-31]. Table 3 summarizes the former papers on the control size of iron oxide particles by adjusting the precursor types and precursor concentration in different spray pyrolysis process, respectively [32-36]. As seen different types of iron compounds such as $Fe(CO)_5$, $Fe(NO_3)_3$, $FeSO_4$, $FeCl_3$ are suitable for the production of iron oxide particles in the spray pyrolysis method.

Table 3. Previous experimental results of iron oxide particles synthesized by different spray pyrolysis methods.

Morphology	Particle size, nm	Precursor salt	Precursor concentration (M)	Heating temperature (°C)	References
Spherical	3-12	$Fe(CO)_5$	-	2150-2450	Kumfer al. [32]
	70 -675	$Fe(NO_3)_3$. 9H2O/ methanol	1.28	500–1100	Ozcelik et al. [33]
	18-33 (crystalline size)	$FeCl_3{\cdot}6H_2O$	0.1	200-600	Gurmen et al. [34]
	16 – 18	$FeCl_3.6H_2O$ /$FeSO_4 \cdot 7H_2O$	-	100-550	Grabıs et al. [35]
	280-560	$Fe(NO_3)_3{\cdot}9(H_2O)$	0.02 -0.2	500	Overcash et al. 36]

In this study, the synthesis of metal and metal oxide nanoparticles; specifically, Ag, Fe_2O_3 and TiO_2 were investigated in an induction system to optimize process conditions with a desired-uniform morphology and particle size distribution. This nanoparticle production system was developed by our research group and consisted of a medium frequency induction furnace and a high frequency ultrasonic spray to facilitate the manufacture of different metal and metal oxide nanoparticles.

Generally, aerosol-based production systems provide a submicron and/or nano particle synthesis with a spherical shape. Besides, the manufacturing of nano particles with these types of techniques from all soluble or organometallic compounds is relatively easier and suitable for implementing mass production compared to the other developed methods; suggested previously [3-9]. Considering the fact that, we had rather to use an aerosol-based production technique in the synthesis of nano particles. In our design, initial solutions were performed by a powerful source of ultrasound to form aerosols with a uniform droplet size. During thermal decomposition stage, the produced aerosols were transported through the inductively heated hot zone via carrier gas, and dried/evaporated then subsequently thermolysed in a single-step. In the induction heating system, the samples to be heated never come into direct contact with a flame or other heating elements; the heat is induced straight on the samples by alternating electrical current. Consequently, spherical, solid, either submicronic or nanoscaled particles are able to be obtained with a continuous process.

The benefit of our preferred fabrication technique is the usage of an induction heating which offers a steady nanoparticle synthesis with a reduced energy consumption, low chemical consumption and maximum product quality.

The purpose of the investigation is to explore nanoparticle production via a medium frequency induction system. For this reason, three different nanoparticles were produced and analyzed via XRD and SEM in order to inspect the purity, size as well as morphology of produced nanoparticles.

2. MATERIALS AND METHODS

2.1. Materials

All Iron Chloride ($FeCl_3.6H_2O$, 97 % pure), Silver Nitrate ($AgNO_3$, 99 % pure), titanium tetra iso-propoxide (TTIP, 95 % pure) were purchased from Merck. All the reagents were used without any further purification. The utilized water was deionized and distilled.

2.2. Methods

For the production of Fe_2O_3 and Ag particles, the solutions of iron chloride and silver nitrate were prepared by dissolving the appropriate amount of $FeCl_3$ and $AgNO_3$ salts in 100 ml distilled water, respectively. All solutions were stirred for 15 min. by using a magnetic stirrer to ensure their homogeneities.

The solution of TTIP salt was utilized as a starting material for the TiO_2 particle production. Since the TiO_2 white powder precipitation occurs very fast between TTIP and deionized water, the stabile solution was prepared with 10 ml HNO_3 addition in order to prevent coarse TiO_2 deposits.

The schematic depiction of the nanoparticle production setup was given in Fig. 1. The developed design consisted of three major units: (1) a high frequency ultrasonic spray for the aerosol generation of particles from their solutions, (2) a medium frequency induction reactor for the thermal decomposition of relevant aerosols and (3) particle collection bottles for the accumulation of the produced nanoparticles.

Due to the superiority of ultrasonic spray system in which a well solubility and hence homogeneity of aerosol generation was enabled, basic soluble chemical compounds were preferred in experimental studies instead of expensive and volatile organometallic ones. Silver nitrate ($AgNO_3$), Iron (III) chloride ($FeCl_3$) and titanium tetra iso-propoxide ($Ti[OCH(CH_3)_2]_4$) were utilized as the starting solutions of silver, iron and titanium, respectively. Firstly, prepared solutions with the desired concentrations were atomized by using a high frequency ultrasonic generator (1.7 MHz), then transported through 800 ºC heated induction reactor (30 kW, 50 kHz frequency, 330 mm length, 24 mm diameter) with the help of carrier gas (air).

During the nanoparticle production, the precursor solution was decomposed into the inductively heated zone in order to form silver, whereas reacted with oxygen to form Fe_2O_3 and TiO_2 particles.

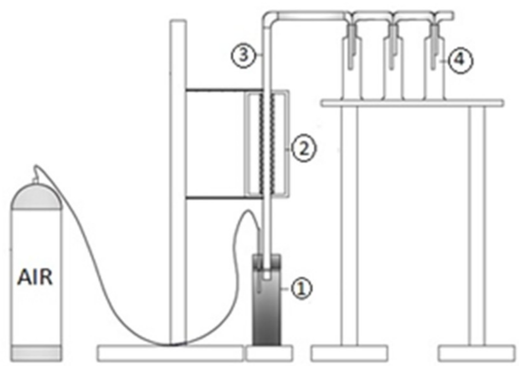

Figure 1. Schematic drawing of the experimental set-up (1-Ultrasonic generator, 2-Inductive reactor, 3- Quartz tube, 4- Powder collectors)

Thermal properties of the reagents ($AgNO_3$ and titanium tetra iso-propoxide; TTIP) were examined in a TA^{TM} Instruments SDT Q600 differential scanning calorimeter (TG/DSC) by placing 15 mg of powders in an alumina crucible and heating them up to 1000 ˚C at a rate of 20 °C/min under nitrogen atmosphere.

The crystal structures of synthesized particles were identified by X-ray diffraction (XRD, Philips 1700 diffractometer) using Cu Kα radiation (λ=1.54187 Å, 2θ range 10°-90°). For XRD analysis, the particles were placed on a glass substrate and allowed to dry in air at room temperature. The morphology and size of produced samples were inspected by utilizing a field emission scanning electron microscopy (FE-SEM, Jeol JSM 700F). The geometric mean diameter and standard deviation were calculated from SEM photos using Leica image manager software.

The process conditions of nanoparticle production experiments were summarized in Table 4.

3. RESULTS AND DISCUSSION

3.1.Thermodynamic Analysis of Precursor Materials

Thermogravimetric (TG) analysis technique was utilized to determine the thermal behaviour of the precursor materials. $AgNO_3$, $FeCl_3.6H_2O$ and TTIP were used in this characterization. TG curves of these raw materials were examined in this part of the investigation. The possible decomposition reactions were proposed with the change of Gibbs free energy calculations carried out by HSC Software program.

Table 4. Composition of precursor solutions and conditions of the production process [($T_{precursor}$=25 °C, solution 100 mL, $T_{heating\ zone}$=800 ºC, flow rate1 L/min.]

Precursor solution	Concentration [mol/l]
($AgNO_3$)	0.1
	0.01
($FeCl_3\cdot 6H_2O$)	0.1
	0.01
(TTIP)	0.1

The thermogravimetric curve of silver nitrate in the temperature ranging from 25 °C to 1000 °C was given in Fig. 2. A major weight loss was seen between 400 °C and 500 °C, and no significant further change was observed.

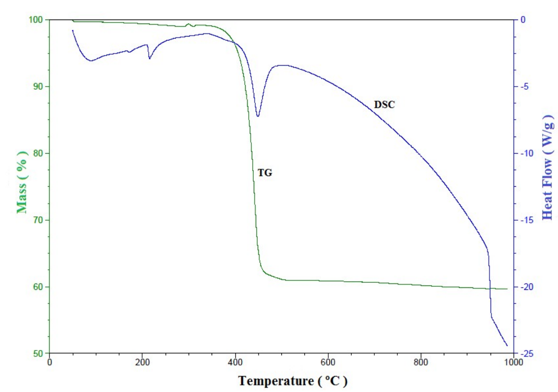

Figure 2. TG/DSC thermograms of $AgNO_3$

The possible thermal decomposition of silver nitrate at 440 °C for the formation of Ag metal could be proposed as in Eq.1.

The values of Gibbs free energy (ΔGº) for the reaction (1) at the temperature range up to 1000 °C confirmed the possibility for the formation of silver by the thermal decomposition of silver nitrate (see Fig3). The Gibbs free energy is positive between 0 ºC and 440 ºC whereas always negative beyond the temperature of 440 °C. Furthermore the curve decreases towards negative values at elevated temperature. It could be deduced that the metallic silver formation by the thermal decomposition of silver nitrate was thermodynamically possible at the desired temperatures between 450 °C and 1000 °C.

$$2AgNO_{3\,(l)} + O_{2\,(g)} = 2Ag_{\,(s)} + 2NO_{2\,(g)} + 2O_{2\,(g)} \qquad (1)$$

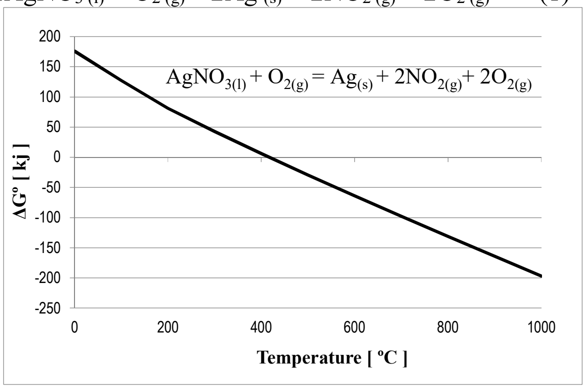

Figure 3. Change of Gibbs free energy for thermal decomposition of silver nitrate

The possible thermal decomposition reaction of iron (III) chloride was given in Eq. 2 with the change of Gibbs free energy diagram (fig. 4). Since the Gibbs free energy of reaction (2) is always negative between 0 °C and 1000 °C, it can be said that the decomposition reaction is likely to occur at the working temperature of 800 °C.

$$2FeCl_{3(l)} + 3/2O_{2(g)} = Fe_2O_{3(s)} + 3Cl_{2(g)} \qquad (2)$$

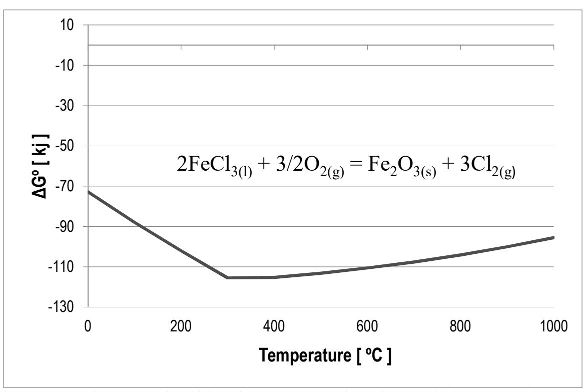

Figure 4. Change of Gibbs free energy for thermal decomposition of iron (III) chloride

Lastly, the thermogravimetric (TG) curve of TTIP at temperatures ranging from 25 to 1000°C was shown in Fig. 5. Apparently, the decomposition of TTIP was completed at around 250 °C.

The stoichiometric reaction for the decomposition of TTIP could be suggested as in Eq.3 [20]

$$(Ti[OCH(CH_3)_2]_4)_{(l)} \rightarrow TiO_{2(s)} + 4C_3H_{6(g)} + 2H_2O_{(g)} \qquad (3)$$

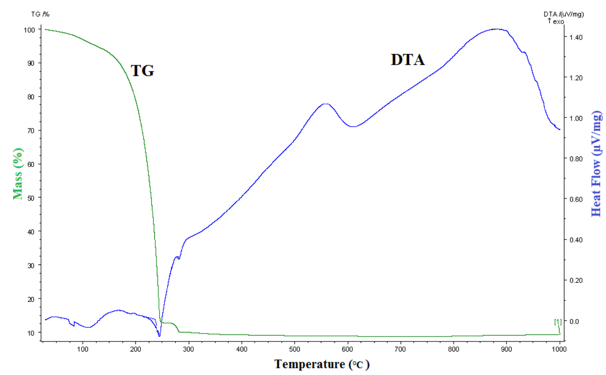

Figure 5. TG/DSC thermograms of TTIP

3.2. The Effect Of Precursor Concentration On The Synthesis of Different Metal / Metal Oxide Nano-Particles

Since the initial solution concentration determinates the amount of metals in the generated aerosols, and hence the transferring quantity to the induction heating zone for nanoparticle production, it is the most critical parameter to be investigated first.

The optimization study of precursor concentrations was carried out at two different concentrations (0.01 and 0.1M) under the constant conditions of 15 min. running time, 800 ºC decomposition temperature, and 1.0 L/min. air volumetric flow rate.

3.2.1 The Effect of Precursor Concentration On Nano-Silver Synthesis

SEM images of the silver particles produced at the concentrations of 0.1 and 0.01 M $AgNO_3$ were given in Fig.6. Apparently, all synthesized silver particles exhibited a perfect spherical morphology with smooth surfaces.

Moreover, the tiny nanoparticles were also detected on the surface of submicron particles as pointed with arrows on the micrograph in Fig 6a. The similar observations were also detected by other researchers [12,13,15]. The possible reason for this type of formation is due to the reaction conditions such as collisions of particles which might lead to break up of primary formed particle clusters.

The synthesized particles at 0.01 M had the perfect spherical morphology with a nanometric size distribution, as seen in Fig. 6c-6d. Magnified SEM images (Fig. 6b and d) revealed the individual existence of particles without any necking formation. Despite the presence of some large particles, as shown in table 5 the general size distribution of particles is relatively narrow.

Based on SEM observations, it could be concluded that the reduction of the precursor concentrations from 0.1 to 0.01 M didn't have any noteworthy influence on the morphology of Ag particle; however, it caused the decrease in the size of particles significantly from approximately 290 nm to 100 nm (see fig. 6 and table 5). The obtained results correspond to those of SHI et al [16].

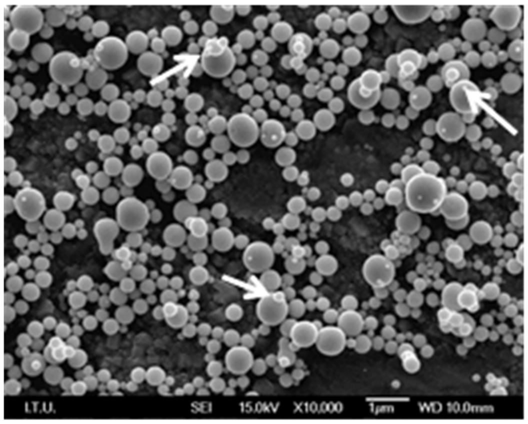

(a)

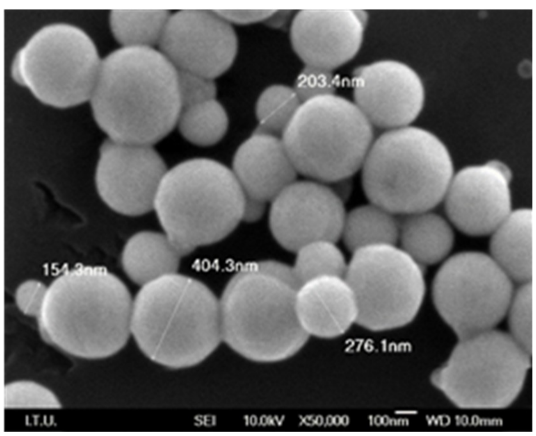

(b)

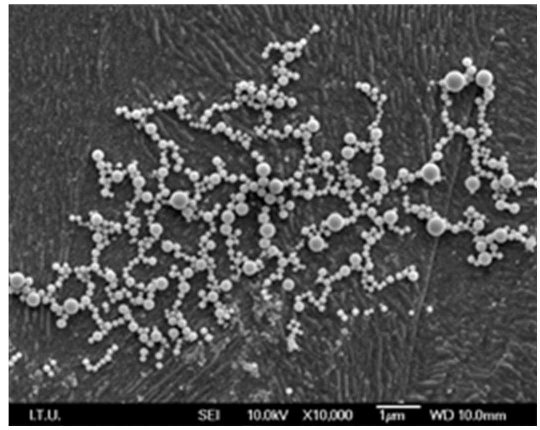

(c)

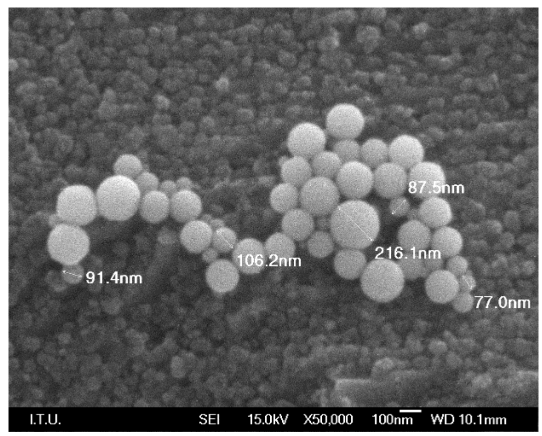

(d)

Figure 6. SEM images of silver particles produced at different $AgNO_3$ concentrations: (a, b) 0.1 mol/L; (c, d) 0.01mol/L

Table 5. Geometric mean particle sizes and standard deviations of Ag particles that calculated using Leica image manager software

Concentration [mol/l]	Mean Particle Size [nm]	Standart Deviation [nm]
0.1 M	290	± 63
0.01 M	100	± 46

XRD investigation of resultant particles confirmed the pure silver nano-powder formation with a face centered cubic structure (JCPDS Card No: 01-004-0783) (fig.7).

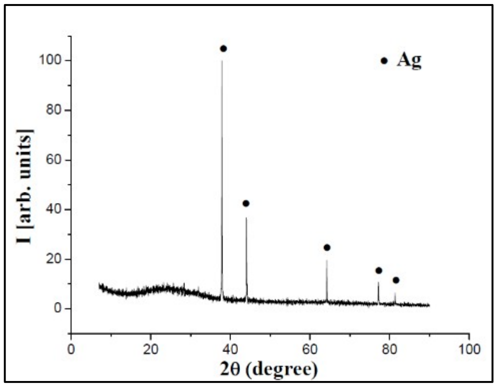

Figure 7. XRD diffraction spectra of nano-Ag particles [0.1 M, 800 ºC, 1 L/min.]

3.2.2 The Effect of Precursor Concentration On Nano-Titanium Dioxide Synthesis

SEM images of TiO_2 particles generated using 0.1 and 0.01 mol/L TTIP precursor concentrations were shown in Fig. 8. Generally, TiO_2 particles have perfect spherical morphology with smooth surfaces. Resembling Fe_2O_3 coarse particles, ultrafine particle formations on the surface of submicron TiO_2 particles were also observed on this particle synthesis (see Fig 10d).

The size distribution of particles was narrow despite the presence of some large particles (see fig. 8a and table 6). The obtained particles were uniform and spherical in shape. The precursor concentration had again a significant effect on the titanium dioxide particles. Particle sizes became coarse by increasing solution concentration, which was typical for the nanoparticle production via aerosol based methods [24].

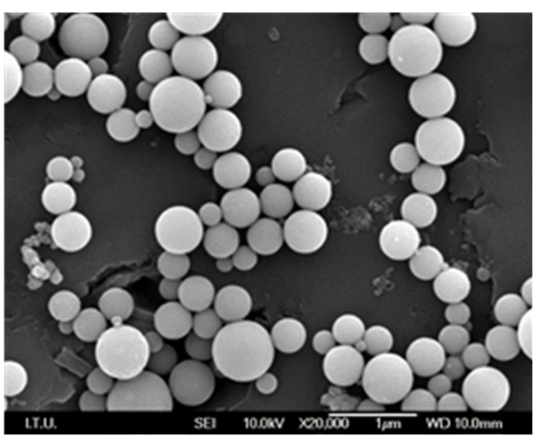

(a)

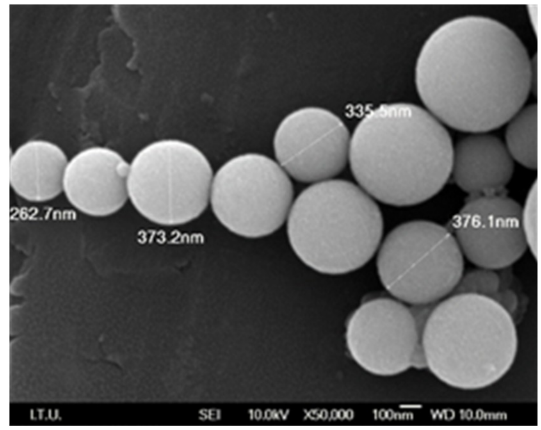

(b)

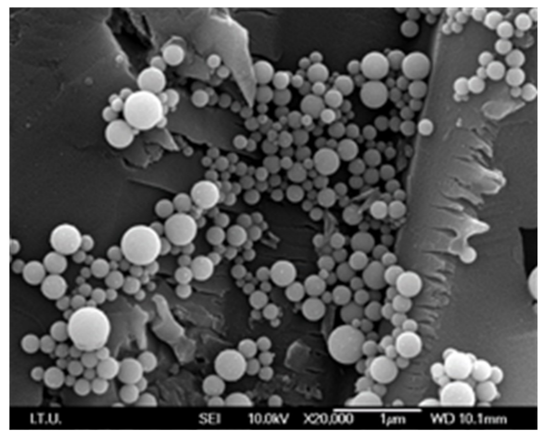

(c)

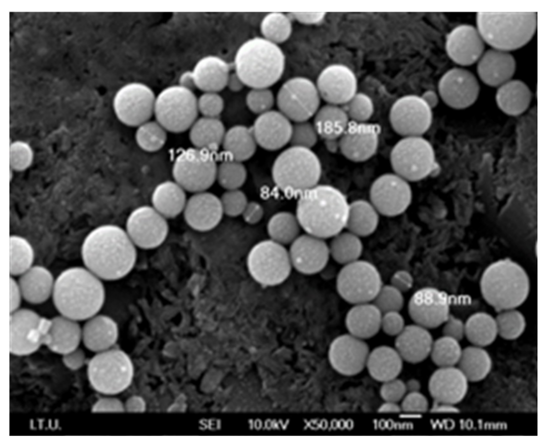

(d)

Figure 8. SEM images of titanium dioxide particles produced at different TTIP concentration: (a, b) 0.1 mol/L; (c, d) 0.01 mol/L

Table 6. Geometric mean particle sizes and standard deviations of TiO_2 particles that calculated using Leica image manager software

Concentration [mol/l]	Mean Particle Size [nm]	Standart Deviation [nm]
0.1 M	350	± 92
0.01 M	150	± 52

XRD study of generated TiO_2 particles revealed the pure TiO_2 formation with an anatase structure. (JCPDS card no. 084-1286) (Fig. 9).

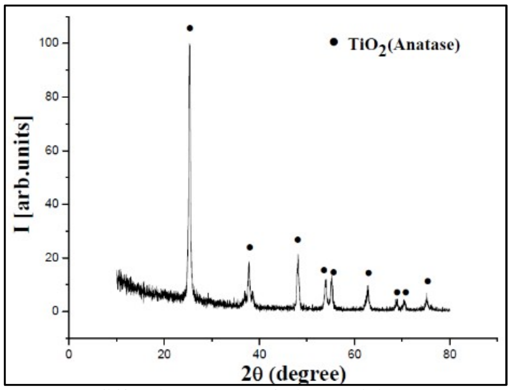

Figure 9. XRD diffraction spectra of TiO_2 particles [0.1 M, 800 ºC, 1 L/min.]

3.2.3.The Effect of Precursor Concentration On Nano-Iron Oxide Synthesis

As generally explained in the introduction part, the transported aerosols were firstly reacted with the carrier gas (air), then nano iron oxide particles nucleated and consequently these nuclei coagulated/condensed in the tubular heated zone. The SEM images of Fe_2O_3 particles produced at the initial concentration of 0.1 M and 0.01 M revealed some coarse particle formations.

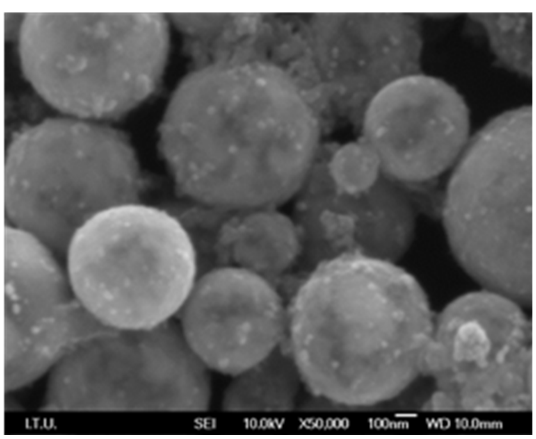

(a)

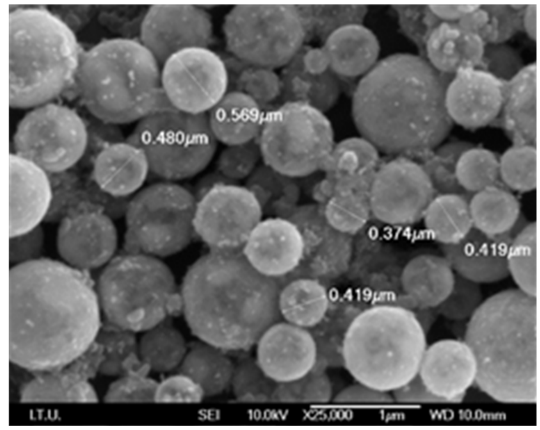

(b)

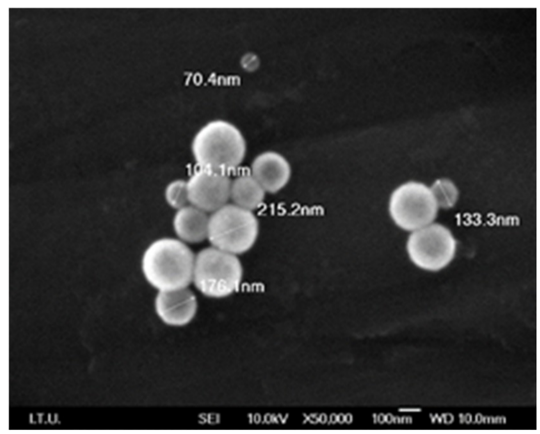

(c)

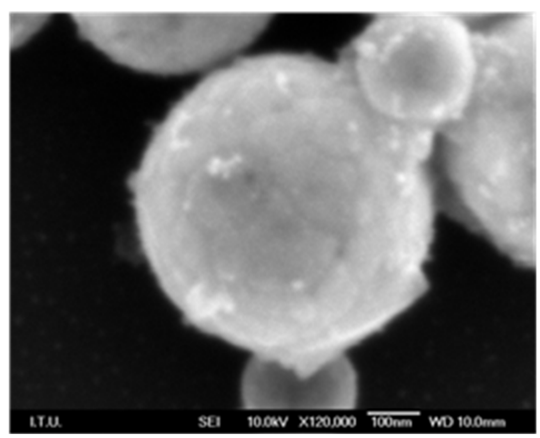

(d)

Figure 10. SEM images of hematite particles produced at different $FeCl_3$ concentrations, (a, b) 0.1 mol/L, (c) 0.01 mol/L, (d) coagulated/agglomerated particles in 0.01 mol/L

The decrease in the concentration of precursor solution caused dramatic decline in the average diameter of the particles. Reducing the solution concentration from 0.1 M to 0.01 M leaded to a decrease in the average particle size from 434 to 170 nm (see Fig. 10b - 10c and table 7). As clearly seen in the higher magnification of SEM image (Fig. 10-d), ultrafine particles were attached to the submicron Fe_2O_3 particles; similar to agglomeration phenomena. The probable reason for this formation is due to the faster agglomeration rate of different particle sizes than that of similar particle sizes. These remarks are in accordance with the study that reported by Gurmen et al [34]. Geometric mean particle sizes and standard deviation values are given in table 7.

Table 7. Geometric mean particle sizes and standard deviations of Fe_2O_3 particles that calculated using Leica image manager software

Concentration [mol/l]	Mean Particle Size [nm]	Standart Deviation [nm]
0.1 M	435	± 163
0.01 M	150	± 55

The XRD pattern of synthesized Fe_2O_3 nanoparticles confirmed rhombohedral Fe_2O_3 phase formation without the presence of any impurities (hematite, JCPDS no. 01-33-0664) (fig. 11).

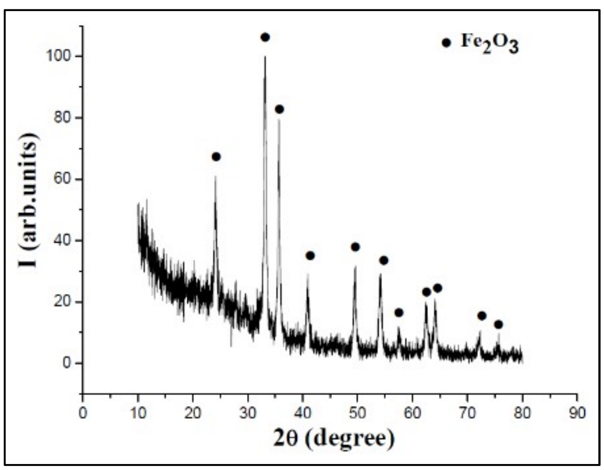

Figure 11.XRD diffraction spectra of Fe_2O_3 particles [0.1 M, 800 ºC, 1 L/min.]

4. CONCLUSION

In this study, an alternative, efficient and continuous production system was proposed to enable the synthesis of uniform nanoparticles. In the experimental design, a high frequency ultrasonic spray and a medium frequency induction heating system were combined to make possible the steady nanoparticle synthesis with the usage of basic chemical compounds. This system was configured with a temperature and a gas flow controller. It was tested by three different kinds of nanoparticles (Ag, Fe_2O_3 and TiO_2). $AgNO_3$, $FeCl_3$ and TTIP were used as starting materials. Based on the reported results, the following conclusions could be drawn:

- This research proved that the necessary energy for the decomposition of precursor material could be easily derivable with an induction system.
- The production of nano-metal/metal oxide particles was achieved from their simple solutions by using the designed induction system with the medium frequency, 50 kHz.
- The size of synthesized particles could be possibly decreased by reducing the molarity of precursor solutions.
- Spherical silver, hematite and titanium dioxide particles could be produced with narrow particle size distribution.
- Finally, the formations of second phase(s) or impurities were not observed in the production of three different nanoparticles. This remark confirmed that the starting materials were sufficiently decomposed to form the nanoparticles at 800 °C decomposition temperature and 1 L/min. volumetric flow rate.

ACKNOWLEDGEMENTS

This research was supported by The Scientific and Technological Research Council of Turkey with Grant No: 110M687.

REFERENCES

[1] R.W. Siegel, “Nanophase Materials: Synthesis, Structure, and Properties’’ in Physics of New Materials F.E. Fujita (Eds.), Springer-Verlag, Berlin Heidelberg, pp. 66-106, 1994.

[2] J. A. Blackman, “Metallic Nanoparticles” in Handbook of Metal Physics, Elsevier B.V, 2009.

[3] N. G. Semaltianos, S. Logothetidis, N. Frangis, I. Tsiaoussis, W. Perrie, G. Dearden, ve K. G. Watkins, “Laser ablation in water: A route to synthesize nanoparticles of titanium monoxide”, Chem. Phys. Lett., cilt 496, no. 1–3, pp.113–116, 2010.

[4] Y. Cheng, S. Choi, ve T. Watanabe, “Effect of nucleation temperature and heat transfer on synthesis of Ti and Fe boride nanoparticles in RF thermal plasmas”, Powder Technol., cilt 246, pp. 210–217.

[5] K. Akurati, A. Vital, G. Fortunato, R. Hany, F. Nueesch, ve T. Graule, ‘Flame synthesis of TiO_2

nanoparticles with high photocatalytic activity', Solid State Sci., cilt 9, no. 3–4, pp. 247–257, 2013.

[6] R. Doong, P.-Y. Chang, ve C. H. Huang, "Microstructural and photocatalytic properties of sol–gel-derived vanadium-doped mesoporous titanium dioxide nanoparticles", J. Non. Cryst. Solids, cilt 355, pp. 2302–2308, 2009.

[7] G. Akgul, F. A. Akgul, K. Attenkofer, ve M. Winterer, "Structural properties of zinc oxide and titanium dioxide nanoparticles prepared by chemical vapor synthesis", J. Alloys Compd., cilt 554, pp. 177–181, 2013.

[8] M. I. Baraton, "Synthesis functionalization and surface treatment of nanoparticles", American Scientific Publishers, California 2003.

[9] W. N. Wang, I. W. Lenggoro, Y. Terashi, T. O. Kim, ve K. Okuyama, "One-step synthesis of titanium oxide nanoparticles by spray pyrolysis of organic precursors", Mater. Sci. Eng. B, cilt 123, no. 3, pp. 194–202, 2005.

[10] M. Ahamed, M. S. Alsalhi, ve M. K. J. Siddiqui, "Silver nanoparticle applications and human health", Clin. Chim. Acta., cilt 411, no. 23-241841-8, 2010.

[11] A. Ravindran, P. Chandran, ve S. S. Khan, "Biofunctionalized silver nanoparticles: advances and prospects", Colloids Surf. B. Biointerfaces, cilt 105, pp. 342–52, 2013.

[12] S. Stopic, P. Dvorak ve B. Friedrich, "Synthesis of spherical nanosized silver powder by ultrasonic spray pyrolysis", Metall, cilt 60, pp. 299–304, 2006.

[13] K. C. Pingali, D. A. Rockstraw, ve S. Deng, "Silver nanoparticles from ultrasonic spray pyrolysis of aqueous silver nitrate", Aerosol Sci. and Technology, cilt 39, no. 10, pp. 1010–1014, 2005.

[14] S. J. Shih ve I-C. Chien, "Preparation and characterization of nanostructured silver particles by one-step spray pyrolysis", Powder Technology, cilt 237, pp. 436–441, 2013.

[15] B. Ebin, E. Yazıcı ve S. Gürmen, "Production of nanocrystalline silver particles by hydrogen reduction of silver nitrate aerosol droplets", Transactions of Nonferrous Metals Society of China, cilt 23, no. 3, pp. 841–848, 2014.

[16] X. Shi, S. Wang, X. Duan, ve Q. Zhang, "Synthesis of nano Ag powder by template and spray pyrolysis technology", Mater. Chem. Phys., cilt 112, no 3, pp. 1110–1113, 2008.

[17] L. Zhanga, M.B. Ranadeb ve J.W. Gentrya, "Synthesis of nanophase silver particles using an aerosol reactor", Aerosol Science, cilt 33, pp. 1559–1575, 2002.

[18] K. H. Lee, S. C. Rah ve S.-G. "Kim, Formation of monodisperse silver nanoparticles in poly(vinylpyrrollidone) matrix using spray pyrolysis", J Sol-Gel Sci Tech., cilt 45, pp. 187-193, 2008.

[19] H.S. Kim, K.-H. Lee ve S.-G.Kim, "Growth of Monodisperse Silver Nanoparticles in Polymer Matrix by Spray Pyrolysis", Aerosol Science and Technology, cilt 40,pp. 536-544, 2006.

[20] Y. Lan, Y. Lu, ve Z. Ren, "Mini review on photocatalysis of titanium dioxide nanoparticles and their solar applications", Nano Energy, cilt 2, pp. 1031–1045, 2013.

[21] J. Yang, X. Zhang, C. Wang, P. Sun, L. Wang, B. Xia, ve Y. Liu, "Solar photocatalytic activities of porous Nb-doped TiO_2 microspheres prepared by ultrasonic spray pyrolysis", Solid State Sci., cilt 14, pp.139–144, 2012.

[22] M. V Liga, E. L. Bryant, V. L. Colvin, and Q. Li, ''Virus inactivation by silver doped titanium dioxide nanoparticles for drinking water treatment'', Water Res., cilt 45, pp. 535–44, 2011.

[23] H. Shi, R. Magaye, V. Castranova, and J. Zhao, ''Titanium dioxide nanoparticles: a review of current toxicological data'', Part. Fibre Toxicology, cilt 10, p. 15. 2013.

[24] W. Wang, I. W. Lenggoroa, Y. Terashib, T. Kimc ve K. Okuyama, ''One-step synthesis of titanium oxide nanoparticles by spray pyrolysis of organic precursors'' Materials Science and Engineering: B, cilt 123, pp. 194–202, 2005.

[25] I. M. Dugandzˇic´, D. J. Jovanovic´, L. T. Mancˇic´,N. Zheng, S.P. Ahrenkiel , O.B. Milosˇevic´, Z. V. S ˇ Aponjic´ ve J. M. Nedeljkovic, "Surface modification of submicronic TiO2 particles prepared by ultrasonic spray pyrolysis for visible light absorption", J Nanopart Res., cilt 14, pp. 1157, 2012.

[26] P. Moravec, J. Smolík, ve V. V. Levdansky, "Preparation of TiO2 fine particles by thermal decomposition of titanium tetraisopropoxide vapor", J. Mater. Sci. Lett.,cilt 20, pp. 2033–2037, 2001.

[27] J. Bogovic, S. Stopic ve B. Friedrich, "Nanosized metallic oxide produced by Ultrasonic Spray Pyrolysis", Proceedings of EMC, 2011.

[28] A. K. Gupta ve M. Gupta, “Synthesis and surface engineering of iron oxide nanoparticles for biomedical applications”, Biomaterials, cilt 26, pp. 3995–4021, 2005.

[29] Z. Cheng, A. L. Kuan Tan, Y. Tao, D. Shan, K. E. Ting, ve X. J. Yin, “Synthesis and characterization of iron oxide nanoparticles and applications in the removal of heavy metals from industrial wastewater”, International Journal of Photoenergy, cilt 2012, 2012.

[30] M. Mohapatra ve S. Anand, “Synthesis and applications of nano-structured iron oxides/hydroxides a review”, Science and Technology, cilt 2, no. 8, pp. 127-146, 2010.

[31] U. Schwertmann ve R. M. Cornell, “The Iron Oxides in the laboratory: preparation and characterization”, Weinheim, Cambridge VCH, pp. 5-18, 1991

[32] B. M. Kumfer, K. Shinoda, B. Jeyadevan ve I. M. Kennedy, “Gas-phase flame synthesis and properties of magnetic iron oxide nanoparticles with reduced oxidation state”, Journal of Aerosol Science cilt 41, pp. 257–265, 2010.

[33] B. K. Ozcelik ve C. Ergun, “Synthesis and characterization of iron oxide particles using spray pyrolysis technique”, Ceramics International, cilt 41, pp. 1994–2005, 2015.

[34] S. Gurmen ve B. Ebin, “Production and characterization of the nanostructured hollow iron oxide spheres and nanoparticles by aerosol route”, Journal of Alloys and Compounds, cilt 492, pp. 585–589, 2010.

[35] J. Grabıs, G. Heıdemane ve D. Rašmane, “Preparation of Fe3O4 and γ-Fe2O3 nanoparticles by liquid and gas phase’’ Processes Materıals Scıence, cilt 14, pp. 292-295, 2008.

[36] J.W. Overcash ve K. S. Suslick, “High surface area iron oxide microspheres via ultrasonic spray pyrolysis of ferritin core analogues”, Chem. Mater., cilt 27, pp. 3564‒3567, 2015.